

Review

Novel Carbon Materials in the Cathode Formulation for High Rate Rechargeable Hybrid Aqueous Batteries

Xiao Zhu, Tuan K. A. Hoang and Pu Chen *

Department of Chemical Engineering and Waterloo Institute for Nanotechnology, University of Waterloo, 200 University Avenue West, Waterloo, ON N2L 3G1, Canada; x58zhu@uwaterloo.ca (X.Z.); tuanchemistry@gmail.com (T.K.A.H.)

* Correspondence: p4chen@uwaterloo.ca; Tel.: +1-519-888-4567 (ext. 35586)

Received: 27 September 2017; Accepted: 8 November 2017; Published: 11 November 2017

Abstract: Novel carbon materials, carbon nanotubes (CNTs) and porous graphene (PG), were exploited and used as conductive additives to improve the rate performance of LiMn_2O_4 cathode for the rechargeable aqueous $\text{Zn}/\text{LiMn}_2\text{O}_4$ battery, namely the rechargeable hybrid aqueous battery (ReHAB). Thanks to the long-range conductivity and stable conductive network provided by CNTs, the rate and cycling performances of LiMn_2O_4 cathode in ReHAB are highly improved—up to about $100 \text{ mAh}\cdot\text{g}^{-1}$ capacity is observed at 10 C ($1 \text{ C} = 120 \text{ mAh}\cdot\text{g}^{-1}$). Except for CNTs, porous graphene (PG) with a high surface area, an abundant porous structure, and an excellent electrical conductivity facilitates the transportation of Li ions and electrons, which can also obviously enhance the rate capability of the ReHAB. This is important because the ReHAB could be charged/discharged in a few minutes, and this leads to potential application of the ReHAB in automobile industry.

Keywords: carbon nanotube; graphene; LiMn_2O_4 ; rechargeable hybrid aqueous battery; high rate capability

1. General Introduction of Aqueous Rechargeable Battery

Batteries are widely used as energy storage systems. Lithium ion batteries can operate at high voltages due to the wide electrochemical stability range of the organic electrolytes (3–5 V vs. Li^+/Li electrode), resulting in high energy densities. Therefore, lithium ion batteries have been widely used in electronic devices and they have been chosen as one of the most promising power sources for electric vehicles (EVs). Unfortunately, these organic electrolytes show high flammability and low ionic conductivity (about two orders of magnitude lower than those of aqueous electrolytes); besides, the fabrication cost of lithium ion batteries is generally high. Aqueous electrolytes are electrochemically stable just in a narrower voltage (1.23 V vs. SHE) than organic electrolytes; however, they are much safer (inherently non-flammable and low toxic) and the fabrication cost of aqueous batteries is much lower than lithium ion batteries, so aqueous batteries are more suitable for low cost and large-scale energy storage [1–3]. Thus far, a variety of aqueous batteries, including alkaline $\text{Zn}-\text{MnO}_2$, lead-acid, Ni-Metal (e.g., zinc, cobalt, and iron), and Ni-metal hydride (Ni-MH) are used extensively or studied widely [1,4–8]. However, these systems also have their own problems. Specifically, the alkaline Zn/MnO_2 is a primary battery, and its disposal causes plenty of pollution to the environment; the poisoning metals of lead and cadmium utilized in lead-acid and Ni-Cd batteries, respectively, may cause damage to the environment; Ni-MH ($\text{M} = \text{La}, \text{Ce}, \text{Nd}, \text{Gd}, \text{etc.}$) batteries utilize rare earth elements, which makes them expensive; and Ni-Co (Fe, Zn) batteries have narrow voltage range.

Recently, a series of aqueous “rocking-chair” batteries based on the ion (e.g., Li^+ , Na^+ , K^+ , and Zn^{2+}) intercalation/de-intercalation processes have been developed [9–20]. In 1994, Dahn et al. first

developed the aqueous $\text{LiMn}_2\text{O}_4/\text{VO}_2$ battery [9], with LiNO_3 solution ($5 \text{ mol}\cdot\text{L}^{-1}$) as the electrolyte. Then, various kinds of aqueous “rocking-chair” lithium ion batteries (e.g., $\text{LiFePO}_4/\text{LiTi}_2(\text{PO}_4)_3$, $\text{LiMn}_2\text{O}_4/\text{LiTi}_2(\text{PO}_4)_3$, and $\text{LiMn}_2\text{O}_4/\text{LiV}_3\text{O}_8$) have been reported; [9–12]. Besides, Cui et al. reported a potassium ion battery, using carbon/polypyrrole hybrid and copper hexacyanoferrate as the anode and the cathode. This battery exhibited an excellent rate capability [14]. Different from aqueous lithium or potassium ion batteries, aqueous sodium ion batteries may be more promising to be used as large-scale energy storage systems due to the rich sodium resources in nature. Whitacre’s and Chiang’s groups both reported aqueous $\text{Na}_{0.44}\text{MnO}_2/\text{NaTi}_2(\text{PO}_4)_3$ batteries [18,19]. However, sodium-intercalated compounds for aqueous systems are limited. Unique Li/Na mixed ion batteries, $\text{Na}_{0.44}\text{MnO}_2/\text{TiP}_2\text{O}_7$ and $\text{LiMn}_2\text{O}_4/\text{Na}_{0.22}\text{MnO}_2$, were developed by Xia’s group, which mainly depend on the intercalation/de-intercalation of Na ions and Li ions, respectively. The specific energy of these two batteries was 25 and 17 $\text{Wh}\cdot\text{kg}^{-1}$, respectively. It is worth mentioning that Li ions and Na ions are separated in aqueous $\text{LiMn}_2\text{O}_4/\text{Na}_{0.22}\text{MnO}_2$ battery due to the special operating mechanism of this system [21]. In addition, Cui et al. found that materials with the Prussian Blue crystal structure (nickel hexacyanoferrate and copper) possess large interstitial sites, which allows for the intercalation/de-intercalation of sodium (potassium) ions [20,22]. Their capacities are between 50 and 60 $\text{mAh}\cdot\text{g}^{-1}$.

2. Introduction of Rechargeable Hybrid Aqueous Battery

New types of aqueous rechargeable batteries, including new electrode materials and chemistry, are required to achieve high power as well as high safety and eco-friendliness. Herein, rechargeable Zn/MnO₂ batteries have been widely studied; however, the redox reactions on the cathode show poor reversibility, which hinders its commercial applications. When electrolytes with $\text{pH} \geq 7$, $\text{Zn}(\text{OH})_2$, ZnO_2^{2-} , and $[\text{Zn}(\text{OH})_4]^{2-}$ are formed depending on potential and pH value, while with $\text{pH} < 7$, $\text{Zn} - 2e^- \rightarrow \text{Zn}^{2+}$ [23]. Minakshi et al. found that replacing MnO₂ by LiMn₂O₄ and changing the electrolyte to aqueous LiOH/ZnSO₄ solution could improve the reversibility; however, due to the high pH value of the electrolyte, only a few amount of cathode material can be used during charge/discharge processes [23]. Recently, Kang et al. developed a mild zinc ion battery, using α -MnO₂ as cathode and Zn as anode [15], which showed high capacities and a high rate capability. Additionally, a new secondary aqueous Zn/LiMn₂O₄ battery system, namely the rechargeable hybrid aqueous battery (ReHAB) has been developed by our group (Figure 1) [24]. The operation of this battery system is based on two different kinds of redox reactions. At the anode, zinc ions are deposited on the zinc sheet and then dissolved into a mild acidic aqueous solution, containing zinc ions, during charge and discharge processes, respectively. At the cathode, Li ions are de-intercalated from and intercalated into LiMn₂O₄ during charge and discharge processes. The advantages of this battery include the capability of functioning at high rate when the cathode formulation is optimized, and the low cost. Most of the materials used in this battery are commercially available. The battery can be assembled under the atmospheric environment.

Table 1 shows the comparison of various types of major secondary aqueous batteries. Among them, lead-acid batteries have the most widely applications [1]. Compared to lead-acid batteries, our ReHAB (Zn/LiMn₂O₄ batteries) shows about doubled energy density and up to 10 times higher cycle life; and is more environmentally friendly; besides, the cost of our ReHAB is almost the same as lead-acid batteries. However, some technical problems must be solved before the commercialization of the ReHAB. The first problem is the rate capability. The capacity of a standard 10 kg ReHAB battery should be about 0.6 kWh. If it could discharge 100% of its capacity at 10 C rate (or 6 min), the power would be high enough to crank a passenger vehicle [25]. To do this, the ReHAB is required to work at 10 C with the specific discharge capacity of not less than $\sim 100 \text{ mAh}\cdot\text{g}^{-1}$. This is accomplished via applying novel carbon materials in the cathode formulation, which is the topic of this review paper. The second problem is the maintenance issue, which we propose to solve by the design of novel thixotropic gel electrolytes [26,27]. The remaining problems are the dendrite formation, corrosion,

and hydrogen gas evolution on the zinc anode [28,29]. Intensive research efforts based on these issues are under progress. With reasonable high energy density, high power, high safety, and low cost, the ReHAB can be exploited as uninterruptible power supplies, large energy storage devices to interface with the grid, and novel start-stop battery in automobile vehicles.

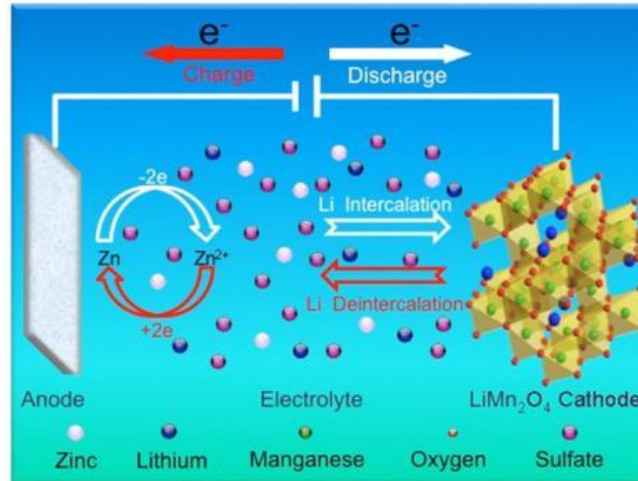


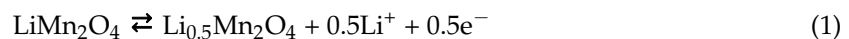
Figure 1. Schematic illustration of the mechanism for ReHAB operation (modified from Ref. [24] with permission from Elsevier).

Table 1. Comparison of various types of major secondary aqueous batteries [1,3,5,16,24].

Type	Ni-Cd Battery	Ni-MH Battery	Aqueous Alkali-Metal Ion Battery	Lead-Acid Battery	Zn/LiMn ₂ O ₄ Battery
Working Voltage (V)	1.2	1.2	1.5	1.8–2.0	1.8
Energy Density (Wh·kg ⁻¹)	30–40	70–80	20–60	30–50	50–80
Power Density (W·kg ⁻¹)	60–90	250–1000	-	250–600	500–800
Cycle Life	<550	500–800	>1000	300–500	1000–4000
Cost (\$·kW·h ⁻¹)	300–600	350–650	-	30–50	30–50

3. Introduction of LiMn₂O₄

Compared with other cathode materials (e.g., LiCoO₂ [30–32], LiNiO₂ [33], LiFePO₄ [34], NaMnO₂ [35] and KMnO₂ [36]) in aqueous rechargeable batteries, spinel LiMn₂O₄ is the most promising cathode material for aqueous rechargeable batteries due to its safety, eco-friendliness, low cost, and excellent structural stability [37]. The crystal structure of spinel LiMn₂O₄, space group *Fd* $\bar{3}$ *m*, is illustrated in Figure 2, in which the Li and Mn cations occupied the 8a tetrahedral and the 16d octahedral sites; Li ions transfer in the three-dimensional (3-D) interstitial space provided by the Mn₂O₄ framework, which can be expressed by Equations (1) and (2) [38,39].



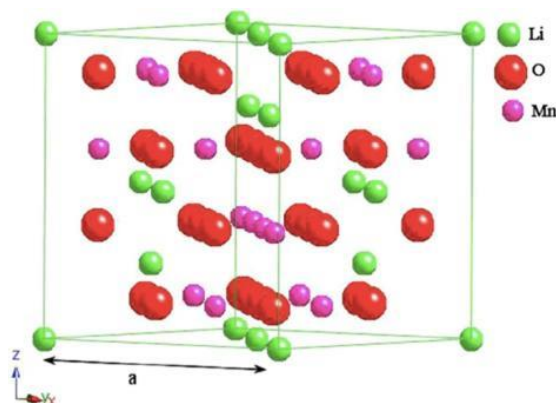


Figure 2. The crystal structure of spinel LiMn_2O_4 (reprinted from Ref. [40] with permission from Elsevier).

In 1994, it was reported that Li ion could de-intercalate/intercalate from/into LiMn_2O_4 in aqueous electrolyte for the first time [9]. In the CV curve of the LiMn_2O_4 in the saturated Li_2SO_4 solution (Figure 3), two pairs of redox peaks at 0.85/0.69 V and 0.98/0.82 V vs. standard calomel electrode (SCE), respectively, represent the two-step de-intercalation/intercalation of Li ions from/into the tunnels of LiMn_2O_4 . Besides, the oxidation potentials are much lower than the oxygen generation potential (~ 1.5 V vs. SCE), revealing the excellent stability of LiMn_2O_4 as the cathode for aqueous rechargeable batteries [41].

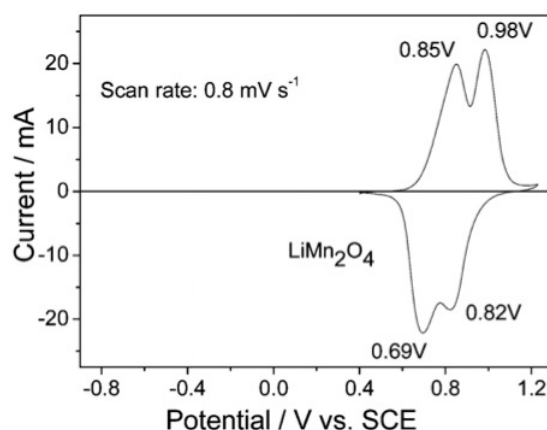


Figure 3. CV curve of the micrometer LiMn_2O_4 in the saturated Li_2SO_4 solution (modified from Ref. [41] with permission from Wiley).

However, the dissolution of Mn^{3+} in acid electrolytes, $\text{Mn}^{3+}_{(\text{solid})} \rightarrow \text{Mn}^{4+}_{(\text{solid})} + \text{Mn}^{2+}_{(\text{liquid})}$, and the phase transition from cubic to tetragonal phase result in the capacity decay, which hindered its practical application [42,43]. The dissolution of Mn^{3+} can be alleviated by surface modification and/or cation doping [38,44–46].

Besides, the rate capability of the LiMn_2O_4 cathode is intrinsically low. Specifically, the diffusion of Li ions and electrons in LiMn_2O_4 is slow, leading to the insufficient Li ion intercalation/de-intercalation under high current density, which cannot satisfy the requirements for energy storage system that can transfer (store or release) energy at high rates [47–49]. Thus, to make the ReHAB capable of working at high rate capability, the development of cathode formulation is one of the most important keys. In this review, we focus on using novel carbon materials, porous graphene and carbon nanotubes (CNTs), as conductive additives to improve the electrical conductivity, thus improving the rate capability of the battery.

4. Increase the Electrical Conductivity of LiMn_2O_4 Cathode by Adding CNTs or Graphene as Conductive Additive

4.1. Increase the Electrical Conductivity of LiMn_2O_4 Cathode by Adding CNTs as Conductive Additive

4.1.1. Structure, Properties and Synthesis of CNTs

Since being discovered by Sumio Iijima in 1991 [50], carbon nanotubes (CNTs) have aroused great interest of researchers. CNTs can be envisaged as cylinders rolled by graphene layers (Figure 4). The length of CNTs ranges from ~ 100 nm to a few centimeters, while the diameter of the hollow cores changes from less than 1 nm to ~ 100 nm, resulting in a high length-to-diameter ratio, or aspect ratio. Based on the number of graphene layers, CNTs can be distinguished into single-walled CNTs (SWNTs) and multi-walled CNTs (MWNTs). SWNTs consist of a single rolled graphene layer, while MWNTs consist of two or more rolled graphene layers [51].

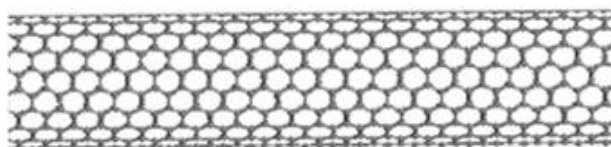


Figure 4. The structural model of carbon nanotube (CNT). (reprinted from Ref. [52] with permission from Elsevier).

CNTs possess unusual properties, including exceptionally high mechanical strength and high electrical conductivity. The bonds of CNTs employ sp^2 -hybrid carbon atoms, which are stronger than the sp^3 -hybrid carbon atoms found in diamond, resulting in amazing mechanical strength of CNTs. The free electrons formed π -electron system, which determines the electronic property; and the one-dimensional (1-D) tube structure facilitates the transport of electrons, which contributes to the high electrical conductivity of CNTs. These unique properties make CNTs be widely used in different kinds of applications, such as nanotechnology, energy storage, electronics, gas storage, water filtration, sensors, and so forth [51,52].

Based on the wide application of CNTs, mass production of CNTs with controlled structures becomes urgent. The techniques usually used to prepare CNTs include arc-discharge [50,53], laser ablation [54], gas-phase pyrolysis [55], and chemical vapor deposition (CVD) [56]. Among these methods, CVD has been used to mass-produce CNTs at a low cost. Wei et al. could produce over thousands of tons of CNTs per year by fluidized bed reactor-based CVD method, with the price of MWNTs below US $\$100 \text{ kg}^{-1}$ and that of SWNTs below US $\$2000 \text{ kg}^{-1}$ [57].

4.1.2. LiMn_2O_4 /CNT Nanocomposites

Recently, LiMn_2O_4 /CNT composites have been prepared by the following methods: mechanical alloying method [58], self-assembly process [59], in-situ hydrothermal method by using MnO_2 /CNT and LiOH as reaction [60–62], microwave-assisted hydrothermal reactions [63,64], spray-deposition method [65] and in-situ hydrothermal growth of binder-free flexible LiMn_2O_4 /CNT composite [63]. These composites have been used in lithium ion batteries as cathode materials, where high electrochemical performances of LiMn_2O_4 were attained.

Additionally, LiMn_2O_4 /CNT composites have been used in aqueous rechargeable batteries. Zhang et al. prepared LiMn_2O_4 /MWNTs composite by a ball-milling process with a high temperature treatment at 500°C for 1 h [66], the morphology of the prepared LiMn_2O_4 /MWNTs composite is shown in Figure 5a. The LiMn_2O_4 /MWNTs cathode was investigated in $1 \text{ mol}\cdot\text{L}^{-1}$ Li_2SO_4 for aqueous rechargeable batteries and it delivered higher discharge capacities than the LiMn_2O_4 cathode at different current densities (Figure 5b). Moreover, the results from electrochemical impedance spectroscopy (EIS) revealed that the transfer of Li ions in the LiMn_2O_4 /MWNTs cathode is much

faster than that in the LiMn_2O_4 cathode. This means that the MWNTs can obviously enhance the capacity storing and the rate capability of the battery. Tang et al. prepared $\text{LiMn}_2\text{O}_4/\text{CNT}$ composite by a hydrothermal method with a heat treatment at $700\text{ }^\circ\text{C}$ for 8 h, the morphology of the prepared $\text{LiMn}_2\text{O}_4/\text{CNT}$ composite is shown in Figure 5c. The $\text{LiMn}_2\text{O}_4/\text{CNT}$ cathode was investigated in $5\text{ mol}\cdot\text{L}^{-1}$ LiNO_3 aqueous electrolyte, and it delivered higher capacities than $\text{LiMn}_2\text{O}_4/\text{active carbon}$ ($\text{LiMn}_2\text{O}_4/\text{AC}$) electrode at different current densities (Figure 5d) [61].

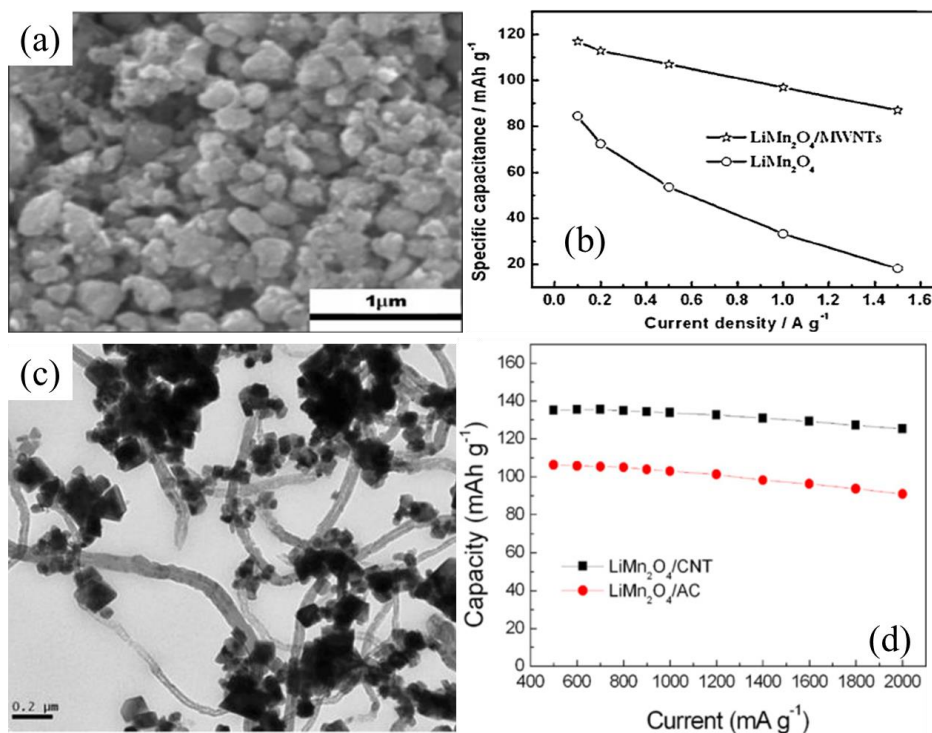


Figure 5. (a) SEM image of as-prepared $\text{LiMn}_2\text{O}_4/\text{MWNTs}$ composite; (b) rate capability of LiMn_2O_4 and $\text{LiMn}_2\text{O}_4/\text{MWNTs}$ in $1\text{ mol}\cdot\text{L}^{-1}$ Li_2SO_4 solution; (c) TEM image of as-synthesized $\text{LiMn}_2\text{O}_4/\text{CNT}$ nanocomposite by hydrothermal reaction; and (d) rate capability for $\text{LiMn}_2\text{O}_4/\text{CNT}$ and $\text{LiMn}_2\text{O}_4/\text{AC}$ composites heat treated at $700\text{ }^\circ\text{C}$ for 8 h (modified from Ref. [61,66] with permission from Springer and Elsevier).

Besides, Dillon's group developed an aqueous paper battery, using LiMn_2O_4 as cathode, carbon coated TiP_2O_7 as anode, and carbon nanotube coated paper as current collector in $5\text{ mol}\cdot\text{L}^{-1}$ LiNO_3 solution [67]. Coated by SWNTs not only reduced the resistance of the paper, but also facilitated the penetration of anode and cathode materials into the conductive substrates, resulting in an improved rate capability in comparison with the organic system.

A three-dimensional carbon nanotube/acetylene black (CNT/AB) network was fabricated and used as conductive additive by our group to improve the rate capability of the LiMn_2O_4 cathode of the rechargeable aqueous $\text{Zn}/\text{LiMn}_2\text{O}_4$ battery system, or ReHAB, using a simple mechanical mixing approach [68]. Figure 6a shows the schematic structure of hierarchical CNT/AB/ LiMn_2O_4 electrodes. The small black dots represent AB nanoparticles, the brown squares represent LiMn_2O_4 nanoparticles, and the blue lines represent CNTs. The morphology of the CNT/AB/ LiMn_2O_4 electrode can also be confirmed by SEM (Figure 6b) and TEM (Figure 6c) images. The CNTs, prepared by a chemical vapor deposition method, show $\sim 100\text{ }\mu\text{m}$ in length and $\sim 11\text{ nm}$ in diameter, which can provide long-range conductive pathways for fast electron transfer. Herein, the CNT/AB/ LiMn_2O_4 electrode (CNT:AB = 1:2, wt %) shows an excellent rate capability (a specific capacity of $105\text{ mAh}\cdot\text{g}^{-1}$ at 10 C, $1\text{ C} = 120\text{ mAh}\cdot\text{g}^{-1}$, Figure 6d).

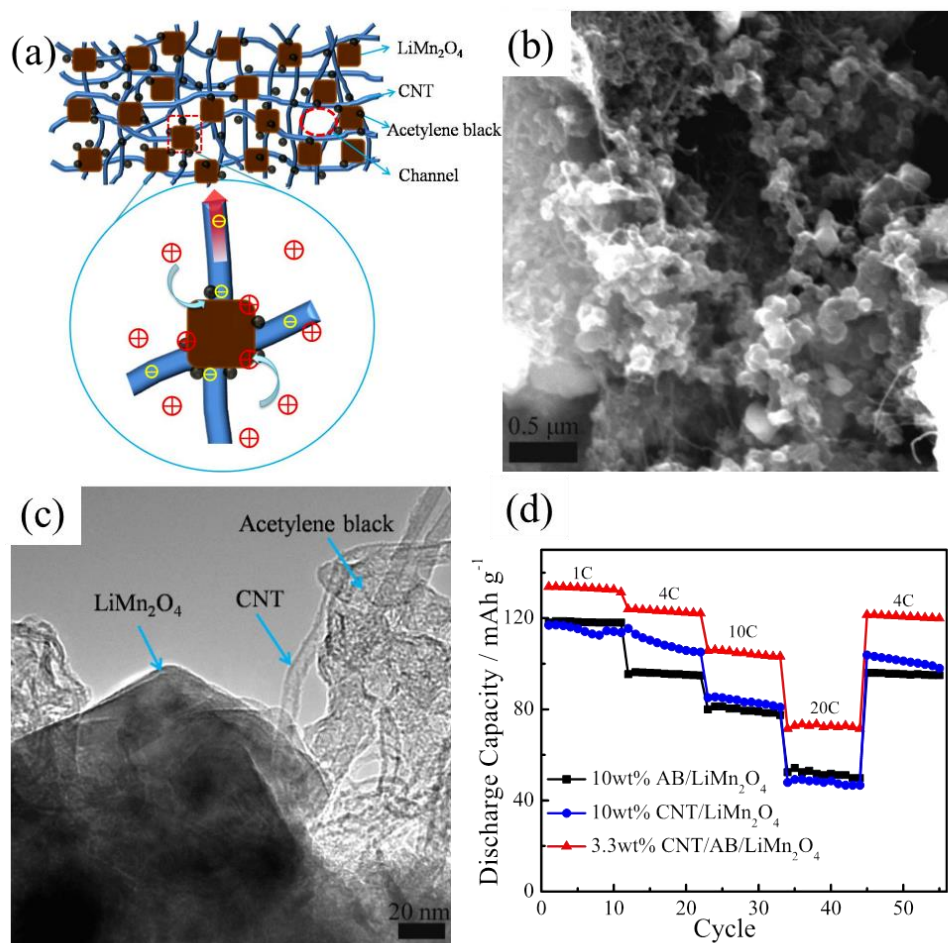


Figure 6. (a) Schematic illustration of CNT/AB/LiMn₂O₄ electrode; (b) SEM; and (c) TEM images of the 3.3 wt % CNT/AB/LiMn₂O₄ electrode; and (d) rate capability of the 3.3 wt % CNT/AB/LiMn₂O₄, 10 wt % CNT/LiMn₂O₄, and 10 wt % AB/LiMn₂O₄ electrodes (modified from Ref. [68] with permission from Springer).

Additionally, a binder-free flexible LiMn₂O₄/CNT hybrid film was prepared by our group (Figure 7a) and used as a high power cathode for the ReHAB [69]. LiMn₂O₄ particles and CNTs are highly entangled together (Figure 7b) to form a free-standing hybrid film with a high mechanical strength (Figure 7c,d) and a good conductivity which facilitate the transfer of electrons. Herein, the LiMn₂O₄/CNT electrode exhibits an excellent rate capability (a specific capacity of 100 mAh·g⁻¹ at 10 C, 1 C = 120 mAh·g⁻¹, Figure 7e). While, the Van Der Waals forces between LiMn₂O₄ nanoparticles and CNTs are weak and these bonding may get weakened during cycling, which results in the minor decrease of capacity (Figure 7f) [70]. It is worth mentioning that this is the first demonstration of using highly stable binder-free flexible LiMn₂O₄/CNT electrodes in aqueous rechargeable battery.

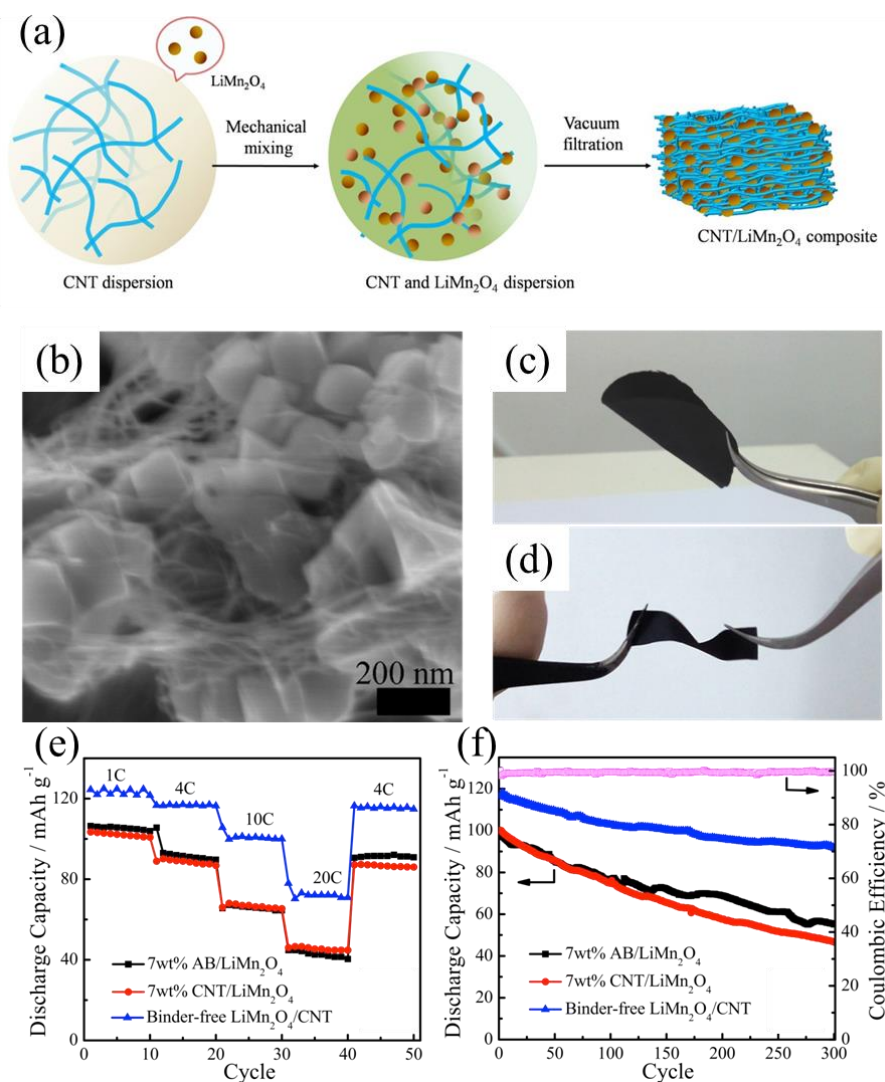


Figure 7. (a) Schematic fabrication of binder-free flexible LiMn₂O₄/CNT network electrodes through dispersion and vacuum filtration processes; (b) SEM image of the binder-free flexible LiMn₂O₄/CNT electrode; optical photographs of the produced hybrid film under: (c) bending; and (d) twisting; and comparison of: (e) rate; and (f) cycling performance of the binder-free LiMn₂O₄/CNT, 7 wt % CNT/LiMn₂O₄, and 7 wt % AB/LiMn₂O₄ electrodes (modified from Ref. [69] with permission from Elsevier).

4.2. Increase the Electrical Conductivity of LiMn₂O₄ Cathode by Adding Graphene as Conductive Additive

4.2.1. Structure, Properties and Synthesis of Graphene

Since being discovered by Geim in 2004, graphene has caused widespread concerns of scientists. Graphene, a two-dimensional (2-D) monolayer graphite sheet of sp² carbon atoms with a honeycomb structure, has a large specific surface area of 2630 m²·g⁻¹ [71,72]. It is considered as the fundamental structural units, which can be wrapped into zero-dimensional (0-D) fullerene, rolled into 1-D CNTs, and stacked into three-dimensional (3-D) graphite, as shown in Figure 8.

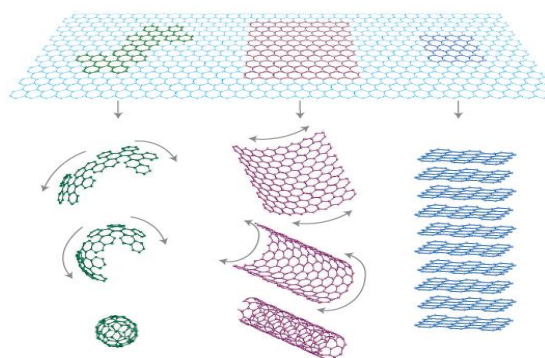


Figure 8. Graphene is the fundamental structural units for other carbonaceous materials (0-D fullerenes, 1-D CNTs and 3-D graphite) (reprinted from Ref. [72] with permission from Nature Publishing Group).

Graphene possesses unique mechanical and thermal properties. The intrinsic tensile strength of graphene is up to 130 GPa, which makes it the strongest material [73]. The thermal conductivity of graphene is up to $5300 \text{ W}\cdot(\text{m}\cdot\text{K})^{-1}$, which is four times of the diamond [74]. Moreover, the highly special electrical properties of graphene attract much more attentions of researchers: the giant intrinsic mobility of which is up to $15,000 \text{ cm}^2\cdot(\text{V}\cdot\text{s})^{-1}$ [75]; the velocity of electrons in which is three hundredth of the speed of light, exceeding most of conductors [76]. All of these electrical properties contribute to the best conductivity of graphene. Graphene is expected to be widely used in different kinds of fields, such as energy storage, nanotechnology, electronic devices, biomedical materials, and so forth [71,77,78].

Currently, there are usually six different methods to prepare graphene: mechanical exfoliation [79], graphene oxide (GO) reduction [80], CVD [81,82], epitaxial growth [83], cutting carbon nanotubes [84], direct sonication and chemical reduction [85]. Among these methods, only GO reduction method and CVD method are suitable for large-scale graphene production.

Li et al. [86] reported the preparation of graphene through a GO reduction method, which includes three steps as following (Figure 9): (1) oxidize graphite to hydrophilic GO with greater interlayer distance by modified Hummers' method; (2) disperse GO in water with ultra-sonication to form GO colloids; (3) convert the insulated GO back to conducted graphene by chemical reduction, for example, using hydrazine. The graphene prepared by the GO reduction method is named as reduced graphene oxide (RGO). The graphene oxide reduction method has inevitable disadvantages: the structure of graphene is destroyed by strong oxidant and reductant used in the preparation process, compromising the electrochemical performance of RGO; besides, graphene oxide is easily accumulated in aqueous solution due to the van der Waals force. However, this method is of low cost and is suitable to prepare graphene derivatives, which expands the application of graphene.

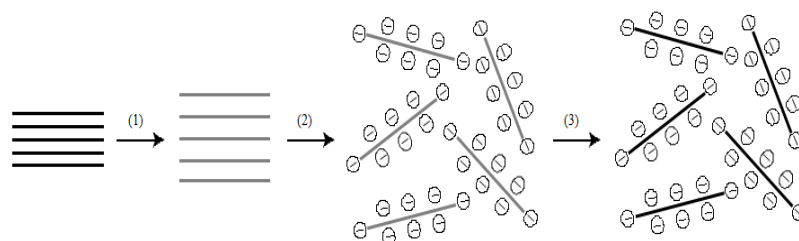


Figure 9. Schematic illustration of the synthesis of reduced graphene oxide dispersions. (1) Graphite (black blocks) is oxidized to graphite oxide (lighter colored blocks) with greater interlayer distance by a modified Hummers' method; (2) Graphite oxide is dispersed in water with an ultra-sonication agitation to form GO colloids; and (3) GO colloids are reduced to reduced graphene oxide (RGO) by hydrazine (reprinted from Ref. [86] with permission from Nature Publishing Group).

The CVD method provides a promising way to realize the controllable preparation of graphene [82]. Graphene with different properties can be obtained by selecting different substrates and carbonaceous sources, as well as controlling reaction temperature in the preparation process. Typically, the substrate (including metal substrates such as Fe, Co, Ni, Cu, etc., and nonmetal substrates such as CuO, NiO, etc.) is exposed to the volatile precursors (usually carbon sources such as acetylene, ethylene, methane, etc.), which cracked at high temperature to form desired deposit on the surface of the substrate. Generally, volatile by-products produced in the CVD process flow out through the reactor. After the substrate is removed, the desired product is obtained.

The ability to form sp^2 crystalline carbon from solid solutions of various transition metals (e.g., Fe, Co, Ni, and Cu) is determined by their carbon affinity [87]. In the case of Fe, the asymmetrical distribution of electrons in the d-shell {[Ar]3d⁶4s²} leads to mutual repulsion, which results in its higher affinity towards carbon [88]; the high affinity between Fe and C makes it more favorable to form carbide than graphitic carbon. Cu has the lowest affinity to carbon [89,90] and has very low carbon solubility compared to Co and Ni (0.001–0.008 wt % at ~1084 °C for Cu [90,91], ~0.6 wt % for Ni at ~1326 °C, and ~0.9 wt % for Co at ~1320 °C) [92], which can owe to the fully filled 3d-electron shell {[Ar]3d¹⁰4s¹} structure of Cu, the most stable configuration; hence, Cu can only form soft bonds with carbon via charge transfer from the p electrons in the sp^2 hybridized carbon to the empty 4s states of Cu [88,93]. Therefore, the very low affinity between carbon and Cu along with the ability to form intermediate soft bonds makes copper the most suitable catalyst for graphitic carbon formation.

Ning et al. prepared a kind of porous graphene, or PG, by CVD method, using porous MgO as substrates. Figure 10 shows the two-step preparation process of PG, synthesis of porous MgO layers and template growth of PG [82]. Firstly, MgO powder was mixed with deionized water under super-ultrasonic stirring. The mixture was boiled in a reflux apparatus for 24 h. After filtration, drying, and calcination at 500 °C for 30 min, porous MgO layers were obtained. Then, PG was prepared by a one-step CVD process, in which CH₄ was cracked at 875 °C to create carbon deposits on the MgO templates, after removing MgO by an acid washing process and drying at 80 °C for 12 h, PG was finally obtained.

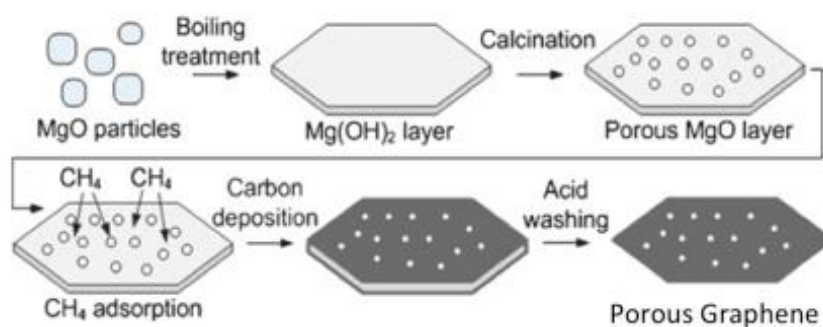


Figure 10. Schematic illustration of the preparation of porous graphene (modified from Ref. [82] with permission from Royal Society of Chemistry).

4.2.2. LiMn₂O₄/Graphene Nanocomposites

Except for CNTs, graphene, a 2-D single layer of carbon atoms, possesses unique properties such as high surface area and superior electrical conductivity [94]. The high surface area can increase the interfacial contact between electrode and electrolyte, resulting in a fast transportation of Li ions; the superior electrical conductivity contributes to a fast electron transport. Therefore, graphene can also be used as an ideal conductive additive to improve the electrochemical performance of LiMn₂O₄ cathode [59,95,96]. Recently, LiMn₂O₄/graphene [97,98] and LiMn₂O₄/RGO [99,100] composites have been prepared and studied as the cathodes of lithium ion batteries, resulting into highly improved rate capabilities.

Additionally, there are a few reports about using graphene in aqueous rechargeable battery [97,101–103]. Jiang et al. used reduced graphene oxide (RGO) nanosheets (inserted figure of Figure 11a) as conductive additive to improve the rate capability of the LiMn_2O_4 cathode. The electrochemical measurements were conducted in $5 \text{ mol}\cdot\text{L}^{-1}$ LiNO_3 aqueous electrolyte. When RGO nanosheets and acetylene black (AB) nanoparticles co-existed with the weight ratio of 1:2 (the content of RGO is 5 wt %, Figure 11a) in the electrode, the rate performance of the LiMn_2O_4 electrode was highly enhanced (Figure 11b). The effective conducting pathways formed by RGO nanosheets and acetylene black nanoparticles contribute to the high rate capability [97].

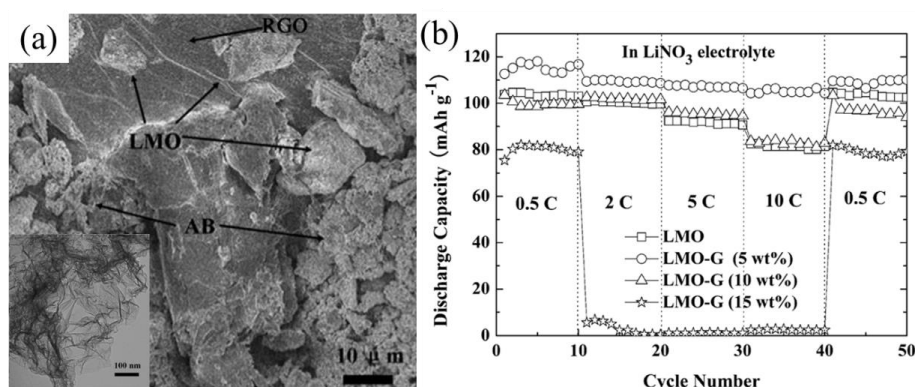


Figure 11. (a) SEM image of the LiMn_2O_4 -RGO (5 wt %), inserted figure shows the TEM image of the RGO; and (b) galvanostatic charge/discharge curves of LiMn_2O_4 -RGO (5 wt %) at various C-rates (modified from Ref. [97] with permission from Royal Society of Chemistry).

Besides, PG was prepared and directly used in our ReHAB as conductive additive in the LiMn_2O_4 cathode [104]. The PG can provide facile access for the electrolyte and high electrical conductivity for the cathode. When mixed with AB with the weight ratio of 1:2 (the content of PG is 3.3 wt %) in the electrode, it also shows a higher rate capability (a specific capacity of $94 \text{ mAh}\cdot\text{g}^{-1}$ at 10 C, $1 \text{ C} = 120 \text{ mAh}\cdot\text{g}^{-1}$), which is comparable to the results of Jiang et al.

4.3. Comparison of Different Conductive Additives in LiMn_2O_4 Cathodes in Aqueous Batteries

The electrochemical performances of LiMn_2O_4 cathodes with different conductive additives in aqueous batteries are listed in Table 2. It shows that better rate capability can be achieved by using CNTs as conductive additive than graphene. Among which, the 3.3 wt % CNT/AB/ LiMn_2O_4 and binder-free flexible LiMn_2O_4 /CNT electrodes prepared by our group both exhibit high rate capability, which attributes to the long-range conductivity provided by CNTs. Although LiMn_2O_4 /CNT composite [61] prepared by a hydrothermal method shows a higher capacity than our electrodes, its content of conductive additive is as high as ~33 wt %, including ~13 wt % CNTs and 20 wt % acetylene black, while, for our electrodes, the content of conductive additive is only 10 wt %, especially for the 3.3 wt % CNT/AB/ LiMn_2O_4 electrode, only 3.3 wt % CNTs was used. Besides, the 3.3 wt % CNT/AB/ LiMn_2O_4 electrode was prepared by a simple mechanical mixing method, which is very simple and feasible to large scale industry applications. Compared to the 3.3 wt % CNT/AB/ LiMn_2O_4 electrode, the 3.3 wt % PG/AB/ LiMn_2O_4 electrode prepared by the same mechanical mixing method shows a much better cycling performance (17% higher capacity retention after 300 cycles at 4 C).

Table 3 compares the properties of different conductive additives, AB, CNTs, and PG, used in the formulation of the LiMn_2O_4 cathode in the ReHAB. Compared to AB, CNTs can provide long-range conductivity; PG with a large surface area can provide a large conducting contact area between LiMn_2O_4 and conducting pathways. However, for CNTs, the reaction between CNTs and Li ions during cycling processes makes them more fragile, so they may break into shorter lengths with the

volume changes of the active materials, resulting in the destroy of the long-range conductivity, thus the decrease of capacity [51]; for the PG, the high cost hinders its large-scale application.

Table 2. Comparison of different conductive additives in LiMn_2O_4 cathodes in aqueous batteries.

Cathode	Specific Capacity at 4 C ($\text{mAh}\cdot\text{g}^{-1}$)	Specific Capacity at 10 C ($\text{mAh}\cdot\text{g}^{-1}$)	Cycling Performance	Reference
$\text{LiMn}_2\text{O}_4/\text{MWNTs}$	110	90	1000 (93%)	[66]
$\text{LiMn}_2\text{O}_4/\text{CNT}$	136	130	2000 (72%)	[61]
3.3 wt % CNT / AB/ LiMn_2O_4	125	105	300 (70%)	[68]
Binder-free flexible $\text{LiMn}_2\text{O}_4/\text{CNT}$	120	100	300 (80%)	[69]
$\text{LiMn}_2\text{O}_4\text{-RGO}$ (5 wt %)	107	105	100 (88%)	[97]
3.3 wt % PG / AB/ LiMn_2O_4	110	94	300 (87%)	[104]

NOTE: MWNTs: Multi-walled Carbon Nanotubes; AB: Acetylene Black; CNTs: Carbon Nanotubes; PG: Porous Graphene; RGO: Reduced Graphene Oxide.

Table 3. Comparison of different conductive additives in LiMn_2O_4 cathode of the ReHAB [104].

Conductive Additive	Specific Surface Area ($\text{m}^2\cdot\text{g}^{-1}$)	Conducting Mode	Price (US: $\text{\$}\cdot\text{kg}^{-1}$)
AB	50–70	Point-to-point	30
CNTs	200–300	Point-to-line	100
PG	1100–1200	Point-to-plane	3000

NOTE: AB: Acetylene Black; CNTs: Carbon Nanotubes; PG: Porous Graphene.

5. Conclusions

This paper gives a review of exploiting CNTs and porous graphene as conductive additives to improve the rate capability of LiMn_2O_4 cathode in the rechargeable aqueous Zn/ LiMn_2O_4 battery, namely the ReHAB. CNTs can provide stable and long-range conducting network, so they can be used as an ideal conductive additive to improve electrical conductivity of battery electrodes. In addition to CNTs, porous graphene with an abundant porous structure, a high surface area, and an excellent electrical conductivity, was used as a conductive additive to the LiMn_2O_4 cathode for the first time, resulting in highly improved electrochemical performance of the LiMn_2O_4 cathode.

CNTs and graphene can highly improve the rate capability of the ReHAB by simple mechanical mixing. Compared to CNTs, LiMn_2O_4 cathode with porous graphene as conductive additive shows much better cycling stability; however, mass production of porous graphene with high quality at a much lower price is still the main problem that hinders its large-scale application; besides, systematic studies of deposition/dissolution rate of zinc at the anode are needed to eliminate its influence on the Li ion diffusion.

Although many obstacles still need to be overcome before the commercialization of the ReHAB, major advances in both performance enhancement and mechanism elucidation of the ReHAB have been reported. It is believed that further investigation will eventually lead to the practical application of the ReHAB in the near future.

Acknowledgments: This research was financially supported by Positec (No. 2100-500-105-2974-121701), the Natural Sciences and Engineering Research Council of Canada (NSERC, No. 216990), Canadian Foundation for Innovation (CFI, No. 202335), the Canada Research Chairs (CRC, No. 211464) program and Mitacs (Nos. IT04444 and IT06145). One of the authors (Xiao Zhu) thanks the China Scholarship Council for Study Abroad Scholarship (No. 201306440001).

Author Contributions: Xiao Zhu wrote the paper; Tuan K. A. Hoang and Pu Chen provided peer review of paper; and Pu Chen provided academic research supervision.

Conflicts of Interest: The authors declare no conflict of interest.

References

1. Soloveichik, G.L. Battery technologies for large-scale stationary energy storage. *Annu. Rev. Chem. Biomol.* **2011**, *2*, 503–527. [[CrossRef](#)] [[PubMed](#)]
2. Wang, F.; Xiao, S.; Hou, Y.; Hu, C.; Liu, L.; Wu, Y. Electrode materials for aqueous asymmetric supercapacitors. *RSC Adv.* **2013**, *3*, 13059. [[CrossRef](#)]
3. Alias, N.; Mohamad, A.A. Advances of aqueous rechargeable lithium-ion battery: A review. *J. Power Sources* **2015**, *274*, 237–251. [[CrossRef](#)]
4. Shen, Y.; Kordesch, K. The mechanism of capacity fade of rechargeable alkaline manganese dioxide zinc cells. *J. Power Sources* **2000**, *87*, 162–166. [[CrossRef](#)]
5. Shukla, A.; Venugopalan, S.; Hariprakash, B. Nickel-based rechargeable batteries. *J. Power Sources* **2001**, *100*, 125–148. [[CrossRef](#)]
6. Köhler, U.; Antonius, C.; Bäuerlein, P. Advances in alkaline batteries. *J. Power Sources* **2004**, *127*, 45–52. [[CrossRef](#)]
7. Wang, H.; Liang, Y.; Gong, M.; Li, Y.; Chang, W.; Mefford, T.; Zhou, J.; Wang, J.; Regier, T.; Wei, F. An ultrafast nickel-iron battery from strongly coupled inorganic nanoparticle/nanocarbon hybrid materials. *Nat. Commun.* **2012**, *3*, 917. [[CrossRef](#)] [[PubMed](#)]
8. Gao, X.P.; Yao, S.M.; Yan, T.Y.; Zhou, Z. Alkaline rechargeable Ni/Co batteries: Cobalt hydroxides as negative electrode materials. *Energy Environ. Sci.* **2009**, *2*, 502–505. [[CrossRef](#)]
9. Li, W.; Dahn, J.; Wainwright, D. Rechargeable lithium batteries with aqueous electrolytes. *Science* **1994**, *264*, 1115–1118. [[CrossRef](#)] [[PubMed](#)]
10. Wang, G.; Fu, L.; Zhao, N.; Yang, L.; Wu, Y.; Wu, H. An aqueous rechargeable lithium battery with good cycling performance. *Angew. Chem. Int. Ed.* **2007**, *119*, 299–301. [[CrossRef](#)]
11. Wang, H.; Huang, K.; Zeng, Y.; Yang, S.; Chen, L. Electrochemical properties of TiP_2O_7 and $\text{LiTi}_2(\text{PO}_4)_3$ as anode material for lithium ion battery with aqueous solution electrolyte. *Electrochim. Acta* **2007**, *52*, 3280–3285. [[CrossRef](#)]
12. Luo, J.Y.; Cui, W.J.; He, P.; Xia, Y.Y. Raising the cycling stability of aqueous lithium-ion batteries by eliminating oxygen in the electrolyte. *Nat. Chem.* **2010**, *2*, 760–765. [[CrossRef](#)] [[PubMed](#)]
13. Wang, X.; Hou, Y.; Zhu, Y.; Wu, Y.; Holze, R. An aqueous rechargeable lithium battery using coated Li metal as anode. *Sci. Rep.* **2013**, *3*, 1401. [[CrossRef](#)] [[PubMed](#)]
14. Pasta, M.; Wessells, C.D.; Huggins, R.A.; Cui, Y. A high-rate and long cycle life aqueous electrolyte battery for grid-scale energy storage. *Nat. Commun.* **2012**, *3*, 1149. [[CrossRef](#)] [[PubMed](#)]
15. Xu, C.; Li, B.; Du, H.; Kang, F. Energetic zinc ion chemistry: The rechargeable zinc ion battery. *Angew. Chem. Int. Ed.* **2012**, *124*, 957–959. [[CrossRef](#)]
16. Whitacre, J.; Tevar, A.; Sharma, S. $\text{Na}_4\text{Mn}_9\text{O}_{18}$ as a positive electrode material for an aqueous electrolyte sodium-ion energy storage device. *Electrochem. Commun.* **2010**, *12*, 463–466. [[CrossRef](#)]
17. Park, S.I.; Gocheva, I.; Okada, S.; Yamaki, J.I. Electrochemical properties of $\text{NaTi}_2(\text{PO}_4)_3$ anode for rechargeable aqueous sodium-ion batteries. *J. Electrochem. Soc.* **2011**, *158*, A1067–A1070. [[CrossRef](#)]
18. Wu, W.; Mohamed, A.; Whitacre, J.F. Microwave synthesized $\text{NaTi}_2(\text{PO}_4)_3$ anode materials for rechargeable aqueous electrolyte sodium-ion battery. In *Meeting Abstracts*; Electrochemical Society (ECS): Pennington, NJ, USA, 2012; Volume 15, p. 1859.
19. Li, Z.; Young, D.; Xiang, K.; Carter, W.C.; Chiang, Y.M. Towards high power high energy aqueous sodium ion batteries: The $\text{NaTi}_2(\text{PO}_4)_3/\text{Na}_{0.44}\text{MnO}_2$ System. *Adv. Energy Mater.* **2013**, *3*, 290–294. [[CrossRef](#)]
20. Wessells, C.D.; Huggins, R.A.; Cui, Y. Copper hexacyanoferrate battery electrodes with long cycle life and high power. *Nat. Commun.* **2011**, *2*, 550. [[CrossRef](#)] [[PubMed](#)]
21. Chen, L.; Gu, Q.; Zhou, X.; Lee, S.; Xia, Y.; Liu, Z. New-concept batteries based on aqueous Li^+/Na^+ mixed-ion electrolytes. *Sci. Rep.* **2013**, *3*, 1946. [[CrossRef](#)] [[PubMed](#)]
22. Wessells, C.D.; Peddada, S.V.; McDowell, M.T.; Huggins, R.A.; Cui, Y. The effect of insertion species on nanostructured open framework hexacyanoferrate battery electrodes. *J. Electrochem. Soc.* **2012**, *159*, A98. [[CrossRef](#)]
23. Minakshi, M.; Singh, P.; Thurgate, S.; Prince, K. Electrochemical behavior of olivine-type LiMnPO_4 in aqueous solutions. *Electrochem. Solid-State Lett.* **2006**, *9*, A471–A474. [[CrossRef](#)]

24. Yan, J.; Wang, J.; Liu, H.; Bakenov, Z.; Gosselink, D.; Chen, P. Rechargeable hybrid aqueous batteries. *J. Power Sources* **2012**, *216*, 222–226. [CrossRef]
25. USABC 12V Start-Stop Battery Goals. Available online: http://www.uscar.org/guest/article_view.php?articles_id=85 (accessed on 27 September 2017).
26. Hoang, T.K.A.; Doan, T.N.L.; Cho, J.H.; Ying, J.; Su, J.; Lee, C.; Lu, C.; Chen, P. Sustainable gel electrolyte containing pyrazole as corrosion inhibitor and dendrite suppressor for aqueous Zn/LiMn₂O₄ battery. *ChemSusChem* **2017**, *10*, 2816–2822. [CrossRef] [PubMed]
27. Hoang, T.K.A.; Doan, T.N.L.; Lu, C.; Ghaznavi, M.; Zhao, H.; Chen, P. Performance of thixotropic gel electrolytes in the rechargeable aqueous Zn/LiMn₂O₄ battery. *ACS Sustain. Chem. Eng.* **2017**, *5*, 1804–1811. [CrossRef]
28. Sun, K.E.K.; Hoang, T.K.A.; Doan, T.N.L.; Yu, Y.; Zhu, X.; Tian, Y.; Chen, P. Suppression of dendrite formation and corrosion on zinc anode of secondary aqueous batteries. *ACS Appl. Mater. Interfaces* **2017**, *9*, 9681–9687. [CrossRef] [PubMed]
29. Hoang, T.K.A.; Doan, T.N.L.; Sun, K.E.K.; Chen, P. Corrosion chemistry and protection of zinc & zinc alloys by polymer-containing materials for potential use in rechargeable aqueous batteries. *RSC Adv.* **2015**, *5*, 41677–41691. [CrossRef]
30. Wang, G.; Qu, Q.; Wang, B.; Shi, Y.; Tian, S.; Wu, Y.; Holze, R. Electrochemical behavior of LiCoO₂ in a saturated aqueous Li₂SO₄ solution. *Electrochim. Acta* **2009**, *54*, 1199–1203. [CrossRef]
31. Wang, G.; Yang, L.; Qu, Q.; Wang, B.; Wu, Y.; Holze, R. An aqueous rechargeable lithium battery based on doping and intercalation mechanisms. *J. Solid State Electrochem.* **2010**, *14*, 865–869. [CrossRef]
32. Winter, M.; Besenhard, J.O.; Spahr, M.E.; Novak, P. Insertion electrode materials for rechargeable lithium batteries. *Adv. Mater.* **1998**, *10*, 725–763. [CrossRef]
33. Ohzuku, T.; Ueda, A. Solid-state redox reactions of LiCoO₂ ($\bar{R}3m$) for 4 volt secondary lithium cells. *J. Electrochem. Soc.* **1994**, *141*, 2972–2977. [CrossRef]
34. Manickam, M.; Singh, P.; Thurgate, S.; Prince, K. Redox behavior and surface characterization of LiFePO₄ in lithium hydroxide electrolyte. *J. Power Sources* **2006**, *158*, 646–649. [CrossRef]
35. Qu, Q.; Shi, Y.; Tian, S.; Chen, Y.; Wu, Y.; Holze, R. A new cheap asymmetric aqueous supercapacitor: Activated carbon//NaMnO₂. *J. Power Sources* **2009**, *194*, 1222–1225. [CrossRef]
36. Qu, Q.; Li, L.; Tian, S.; Guo, W.; Wu, Y.; Holze, R. A cheap asymmetric supercapacitor with high energy at high power: Activated carbon//K_{0.27}MnO₂·0.6H₂O. *J. Power Sources* **2010**, *195*, 2789–2794. [CrossRef]
37. Qu, Q.; Fu, L.; Zhan, X.; Samuelis, D.; Maier, J.; Li, L.; Tian, S.; Li, Z.; Wu, Y. Porous LiMn₂O₄ as cathode material with high power and excellent cycling for aqueous rechargeable lithium batteries. *Energy Environ. Sci.* **2011**, *4*, 3985–3990. [CrossRef]
38. Shaju, K.M.; Bruce, P.G. A stoichiometric nano-LiMn₂O₄ spinel electrode exhibiting high power and stable cycling. *Chem. Mater.* **2008**, *20*, 5557–5562. [CrossRef]
39. Jiao, F.; Bao, J.; Hill, A.H.; Bruce, P.G. Synthesis of ordered mesoporous Li-Mn-O spinel as a positive electrode for rechargeable lithium batteries. *Angew. Chem. Int. Ed.* **2008**, *47*, 9711–9716. [CrossRef] [PubMed]
40. Xia, H.; Luo, Z.; Xie, J. Nanostructured LiMn₂O₄ and their composites as high-performance cathodes for lithium-ion batteries. *Prog. Nat. Sci.* **2012**, *22*, 572–584. [CrossRef]
41. Wang, G.; Qu, Q.; Wang, B.; Shi, Y.; Tian, S.; Wu, Y. An aqueous electrochemical energy storage system based on doping and intercalation: Ppy//LiMn₂O₄. *ChemPhysChem* **2008**, *9*, 2299–2301. [CrossRef] [PubMed]
42. Lim, S.H.; Cho, J. PVP-assisted ZrO₂ coating on LiMn₂O₄ spinel cathode nanoparticles prepared by MnO₂ nanowire templates. *Electrochem. Commun.* **2008**, *10*, 1478–1481. [CrossRef]
43. Wang, X.; Nakamura, H.; Yoshio, M. Capacity fading mechanism for oxygen defect spinel as a 4 V cathode material in Li-ion batteries. *J. Power Sources* **2002**, *110*, 19–26. [CrossRef]
44. Hernán, L.; Morales, J.; Sánchez, L.; Castellón, E.R.; Aranda, M.A.G. Synthesis, characterization and comparative study of the electrochemical properties of doped lithium manganese spinels as cathodes for high voltage lithium batteries. *J. Mater. Chem.* **2002**, *12*, 734–741. [CrossRef]
45. Gnanaraj, J.S.; Pol, V.G.; Gedanken, A.; Aurbach, D. Improving the high-temperature performance of LiMn₂O₄ spinel electrodes by coating the active mass with MgO via a sonochemical method. *Electrochem. Commun.* **2003**, *5*, 940–945. [CrossRef]

46. Arumugam, D.; Kalaiganan, G.P. Synthesis and electrochemical characterizations of nano-La₂O₃-coated nanostructure LiMn₂O₄ cathode materials for rechargeable lithium batteries. *Mater. Res. Bull.* **2010**, *45*, 1825–1831. [[CrossRef](#)]
47. Tarascon, J.M.; Armand, M. Issues and challenges facing rechargeable lithium batteries. *Nature* **2001**, *414*, 359–367. [[CrossRef](#)] [[PubMed](#)]
48. Armand, M.; Tarascon, J.M. Building better batteries. *Nature* **2008**, *451*, 652–657. [[CrossRef](#)] [[PubMed](#)]
49. Kim, T.H.; Park, J.S.; Chang, S.K.; Choi, S.; Ryu, J.H.; Song, H.K. The current move of lithium ion batteries towards the next phase. *Adv. Energy Mater.* **2012**, *2*, 860–872. [[CrossRef](#)]
50. Iijima, S. Helical microtubules of graphitic carbon. *Nature* **1991**, *354*, 56–58. [[CrossRef](#)]
51. Jia, X.; Wei, F. Advances in production and applications of carbon nanotubes. *Top. Curr. Chem.* **2017**, *375*, 18. [[CrossRef](#)] [[PubMed](#)]
52. Liu, X.M.; Huang, Z.D.; Oh, S.W.; Zhang, B.; Ma, P.C.; Yuen, M.M.F.; Kima, J.K. Carbon nanotube (CNT)-based composites as electrode material for rechargeable Li-ion batteries: A review. *Compos. Sci. Technol.* **2012**, *72*, 121–144. [[CrossRef](#)]
53. Journet, C.; Maser, W.K.; Bernier, P.; Loiseau, A.; de la Chapelle, M.L.; Lefrant, S.; Deniard, P.; Lee, R.; Fischer, J.E. Large scale production of single-walled carbon nanotubes by the electric-arc technique. *Nature* **1997**, *388*, 756–758. [[CrossRef](#)]
54. Rinzler, A.G.; Liu, J.; Dai, H.; Nikolaev, P.; Huffman, C.B.; Rodríguez-Macías, F.J.; Boul, P.J.; Lu, A.H.; Heymann, D.; Colbert, D.T.; et al. Large-scale purification of single-wall carbon nanotubes: Process, product, and characterization. *Appl. Phys. A* **1998**, *67*, 29–37. [[CrossRef](#)]
55. Pavel, N.; Bronikowski, M.J.; Bradley, R.K.; Rohmund, F.; Colbert, D.T.; Smith, K.A.; Smalley, R.E. Gas-phase catalytic growth of single-walled carbon nanotubes from carbon monoxide. *Chem. Phys. Lett.* **1999**, *313*, 91–97. [[CrossRef](#)]
56. Ren, Z.F. Synthesis of large arrays of well-aligned carbon nanotubes on glass. *Science* **1998**, *282*, 1105–1107. [[CrossRef](#)] [[PubMed](#)]
57. Zhang, Q.; Huang, J.Q.; Qian, W.Z.; Zhang, Y.Y.; Wei, F. The road for nanomaterials industry: A review of carbon nanotube production, post-treatment, and bulk applications for composites and energy storage. *Small* **2013**, *8*, 1237–1265. [[CrossRef](#)] [[PubMed](#)]
58. Guler, M.O.; Akbulut, A.; Cetinkaya, T.; Akbulut, H. The effect of MWCNT reinforcing on the electrochemical performance of LiMn₂O₄/MWCNT nanocomposite cathodes. *Int. J. Energy Res.* **2014**, *38*, 509–517. [[CrossRef](#)]
59. Zhao, X.; Hayner, C.M.; Kung, H.H. Self-assembled lithium manganese oxide nanoparticles on carbon nanotube or graphene as high-performance cathode material for lithium-ion batteries. *J. Mater. Chem.* **2011**, *21*, 17297–17303. [[CrossRef](#)]
60. Ding, Y.; Li, J.; Zhao, Y.; Guan, L. Direct growth of LiMn₂O₄ on carbon nanotubes as cathode materials for lithium ion batteries. *Mater. Lett.* **2012**, *68*, 197–200. [[CrossRef](#)]
61. Tang, M.; Yuan, A.; Zhao, H.; Xu, J. High-performance LiMn₂O₄ with enwrapped segmented carbon nanotubes as cathode material for energy storage. *J. Power Sources* **2013**, *235*, 5–13. [[CrossRef](#)]
62. Xia, H.; Ragavendran, K.R.; Xie, J.; Lu, L. Ultrafine LiMn₂O₄/carbon nanotube nanocomposite with excellent rate capability and cycling stability for lithium-ion batteries. *J. Power Sources* **2012**, *212*, 28–34. [[CrossRef](#)]
63. Jia, X.; Yan, C.; Chen, Z.; Wang, R.; Zhang, Q.; Guo, L.; Wei, F.; Lu, Y. Direct growth of flexible LiMn₂O₄/CNT lithium-ion cathodes. *Chem. Commun.* **2011**, *47*, 9669–9671. [[CrossRef](#)] [[PubMed](#)]
64. Ma, S.B.; Nam, K.W.; Yoon, W.S.; Bak, S.M.; Yang, X.Q.; Cho, B.W.; Kim, K.B. Nano-sized lithium manganese oxide dispersed on carbon nanotubes for energy storage applications. *Electrochem. Commun.* **2009**, *11*, 1575–1578. [[CrossRef](#)]
65. Hong, H.P.; Kim, M.S.; Lee, Y.H.; Yu, J.S.; Lee, C.J.; Min, N.K. Spray deposition of LiMn₂O₄ nanoparticle-decorated multiwalled carbon nanotube films as cathode material for lithium-ion batteries. *Thin Sol. Films* **2013**, *547*, 68–71. [[CrossRef](#)]
66. Chen, S.; Mi, C.; Su, L.; Gao, B.; Fu, Q.; Zhang, X. Improved performances of mechanical-activated LiMn₂O₄/MWNTs cathode for aqueous rechargeable lithium batteries. *J. Appl. Electrochem.* **2009**, *39*, 1943–1948. [[CrossRef](#)]
67. Sun, K.; Juarez, D.A.; Huang, H.; Jung, E.; Dillon, S.J. Aqueous lithium ion batteries on paper substrates. *J. Power Sources* **2014**, *248*, 582–587. [[CrossRef](#)]

68. Zhu, X.; Doan, T.N.L.; Yu, Y.; Tian, Y.; Sun, K.E.K.; Zhao, H.; Chen, P. Enhancing rate performance of LiMn_2O_4 cathode in rechargeable hybrid aqueous battery by hierarchical carbon nanotube/acetylene black conductive pathways. *Ionics* **2016**, *22*, 71–76. [[CrossRef](#)]
69. Zhu, X.; Wu, X.; Doan, T.N.L.; Tian, Y.; Zhao, H.; Chen, P. Binder-free flexible LiMn_2O_4 /carbon nanotube network as high power cathode for rechargeable hybrid aqueous battery. *J. Power Sources* **2016**, *326*, 498–504. [[CrossRef](#)]
70. Cheng, Q.; Song, Z.; Ma, T.; Smith, B.B.; Tang, R.; Yu, H.; Jiang, H.; Chan, C.K. Folding paper-based lithium-ion batteries for higher areal energy densities. *Nano Lett.* **2013**, *13*, 4969–4974. [[CrossRef](#)] [[PubMed](#)]
71. Kucinskis, G.; Bajars, G.; Kleperis, J. Graphene in lithium ion battery cathode materials: A review. *J. Power Sources* **2013**, *240*, 66–79. [[CrossRef](#)]
72. Geim, A.K.; Novoselov, K.S. The rise of graphene. *Nat. Mater.* **2007**, *6*, 183–191. [[CrossRef](#)] [[PubMed](#)]
73. Kim, K.J.; Lee, H.; Choi, J.; Lee, H.; Kang, T.; Kim, B.; Kim, S. Temperature dependent structural changes of graphene layers on 6H-SiC (0001) surfaces. *Condens. Matter Phys.* **2008**, *20*, 225017. [[CrossRef](#)]
74. Balandin, A.A.; Ghosh, S.; Bao, W.; Calizo, I.; Teweldebrhan, D.; Miao, F.; Lau, C.N. Superior thermal conductivity of single-layer graphene. *Nano Lett.* **2008**, *8*, 902–907. [[CrossRef](#)] [[PubMed](#)]
75. Chen, J.H.; Jang, C.; Xiao, S.; Ishigami, M.; Fuhrer, M.S. Intrinsic and extrinsic performance limits of graphene devices on SiO_2 . *Nat. Nanotechnol.* **2008**, *3*, 206–209. [[CrossRef](#)] [[PubMed](#)]
76. Novoselov, K.S.; Jiang, Z.; Zhang, Y.; Morozov, S.; Stormer, H.; Zeitler, U.; Maan, J.; Boebinger, G.; Kim, P.; Geim, A. Room-temperature quantum Hall effect in graphene. *Science* **2007**, *315*, 1379. [[CrossRef](#)] [[PubMed](#)]
77. Chen, K.S.; Xu, R.; Luu, N.S.; Secor, E.B.; Hamamoto, K.; Li, Q.; Kim, S.; Sangwan, V.K.; Balla, I.; Guiney, L.M.; et al. Comprehensive enhancement of nanostructured lithium-ion battery cathode materials via conformal graphene dispersion. *Nano Lett.* **2017**, *17*, 2539–2546. [[CrossRef](#)] [[PubMed](#)]
78. Jo, G.; Choe, M.; Lee, S.; Park, W.; Kahng, Y.H.; Lee, T. The application of graphene as electrodes in electrical and optical devices. *Nanotechnology* **2012**, *23*, 112001. [[CrossRef](#)] [[PubMed](#)]
79. Novoselov, K.; Jiang, D.; Schedin, F.; Booth, T.; Khotkevich, V.; Morozov, S.; Geim, A. Two-dimensional atomic crystals. *Proc. Natl. Acad. Sci. USA* **2005**, *102*, 10451. [[CrossRef](#)] [[PubMed](#)]
80. Shen, J.; Hu, Y.; Shi, M.; Lu, X.; Qin, C.; Li, C.; Ye, M. Fast and facile preparation of graphene oxide and reduced graphene oxide nanoplatelets. *Chem. Mater.* **2009**, *15*, 3514–3520. [[CrossRef](#)]
81. Fan, Z.; Yan, J.; Ning, G.; Wei, T.; Zhi, L.; Wei, F. Porous graphene networks as high performance anode materials for lithium ion batteries. *Carbon* **2013**, *60*, 558–561. [[CrossRef](#)]
82. Ning, G.; Fan, Z.; Wang, G.; Gao, J.; Qian, W.; Wei, F. Gram-scale synthesis of nanomesh graphene with high surface area and its application in supercapacitor electrodes. *Chem. Commun.* **2011**, *47*, 5976. [[CrossRef](#)] [[PubMed](#)]
83. Iezhokin, I.; Offermans, P.; Brongersma, S.; Giesbers, A.; Flipse, C. High sensitive quasi freestanding epitaxial graphene gas sensor on 6H-SiC. *Appl. Phys. Lett.* **2013**, *103*, 053514. [[CrossRef](#)]
84. Wang, H.; Wang, Y.; Hu, Z.; Wang, X. Cutting and unzipping multiwalled carbon nanotubes into curved graphene nanosheets and their enhanced supercapacitor performance. *ACS Appl. Mater. Interfaces* **2012**, *4*, 6827–6834. [[CrossRef](#)] [[PubMed](#)]
85. Mohammad Choucair, P.T.; John, A. Stride. Gram-scale production of graphene based on solvothermal synthesis and sonication. *Nat. Nanotechnol.* **2009**, *4*, 30–33. [[CrossRef](#)] [[PubMed](#)]
86. Li, D.; Mueller, M.B.; Gilje, S.; Kaner, R.B.; Wallace, G.G. Processable aqueous dispersions of graphene nanosheets. *Nat. Nanotechnol.* **2008**, *3*, 101–105. [[CrossRef](#)] [[PubMed](#)]
87. Mattevi, C.; Kima, H.; Chhowalla, M. A review of chemical vapour deposition of graphene on copper. *J. Mater. Chem.* **2011**, *21*, 3324–3334. [[CrossRef](#)]
88. Earnshaw, A.; Harrington, T.J. *The Chemistry of the Transition Elements*; Oxford University Press: Oxford, UK, 1972.
89. McLellan, R.B. The solubility of carbon in solid gold, copper, and silver. *Scr. Metal.* **1969**, *3*, 389–391. [[CrossRef](#)]
90. López, G.A.; Mittemeijer, E.J. The solubility of C in solid Cu. *Scr. Mater.* **2004**, *51*, 1–5. [[CrossRef](#)]
91. Oshima, C.; Nagashima, A. Ultra-thin epitaxial films of graphite and hexagonal boron nitride on solid surfaces. *J. Phys. Condens. Matter* **1997**, *9*, 1–20. [[CrossRef](#)]
92. Baker, H. ASM International Materials, Alloy Phase Diagrams. In *ASM Handbook*; ASM International Materials: Geauga County, OH, USA, 1992.

93. Sutter, P.; Hybertsen, M.S.; Sadowski, J.T.; Sutter, E. Electronic structure of rew-layer epitaxial graphene on Ru(0001). *Nano Lett.* **2009**, *9*, 2654. [[CrossRef](#)] [[PubMed](#)]
94. Sharma, Y.; Sharma, N.; Rao, G.; Chowdari, B. Li-storage and cyclability of urea combustion derived ZnFe₂O₄ as anode for Li-ion batteries. *Electrochim. Acta* **2008**, *53*, 2380–2385. [[CrossRef](#)]
95. Fu, Y.; Wan, Y.; Xia, H.; Wang, X. Nickel ferrite–graphene heteroarchitectures: Toward high-performance anode materials for lithium-ion batteries. *J. Power Sources* **2012**, *213*, 338–342. [[CrossRef](#)]
96. Wang, Y.; Feng, Z.S.; Chen, J.J.; Zhang, C. Synthesis and electrochemical performance of LiFePO₄/graphene composites by solid-state reaction. *Mater. Lett.* **2012**, *71*, 54–56. [[CrossRef](#)]
97. Jiang, R.; Cui, C.; Ma, H. Using graphene nanosheets as a conductive additive to enhance the rate performance of spinel LiMn₂O₄ cathode material. *Phys. Chem. Chem. Phys.* **2013**, *15*, 6406–6415. [[CrossRef](#)] [[PubMed](#)]
98. Xu, H.; Cheng, B.; Wang, Y.; Zheng, L.; Duan, X.; Wang, L.; Yang, J.; Qian, Y. Improved electrochemical performance of LiMn₂O₄/graphene composite as cathode material for lithium ion battery. *Int. J. Electrochem. Sci.* **2012**, *7*, 10627–10632.
99. Jo, K.Y.; Han, S.Y.; Lee, J.M.; Kim, I.Y.; Nahm, S.; Choi, J.W.; Hwang, S.J. Remarkable enhancement of the electrode performance of nanocrystalline LiMn₂O₄ via solvothermally-assisted immobilization on reduced graphene oxide nanosheets. *Electrochim. Acta* **2013**, *92*, 188–196. [[CrossRef](#)]
100. Bak, S.M.; Nam, K.W.; Lee, C.W.; Kim, K.H.; Jung, H.C.; Yang, X.Q.; Kim, K.B. Spinel LiMn₂O₄/reduced graphene oxide hybrid for high rate lithium ion batteries. *J. Mater. Chem.* **2011**, *21*, 17309–17315. [[CrossRef](#)]
101. Yu, G.; Hu, L.; Vosgueritchian, M.; Wang, H.; Xie, X.; McDonough, J.R.; Cui, X.; Cui, Y.; Bao, Z. Solution-processed graphene/MnO₂ nanostructured textiles for high-performance electrochemical capacitors. *Nano Lett.* **2011**, *11*, 2905–2911. [[CrossRef](#)] [[PubMed](#)]
102. Fan, Z.; Yan, J.; Wei, T.; Zhi, L.; Ning, G.; Li, T.; Wei, F. Asymmetric supercapacitors based on graphene/MnO₂ and activated carbon nanofiber electrodes with high power and energy density. *Adv. Funct. Mater.* **2011**, *21*, 2366–2375. [[CrossRef](#)]
103. Wu, Z.S.; Ren, W.; Wang, D.W.; Li, F.; Liu, B.; Cheng, H.M. High-energy MnO₂ nanowire/graphene and graphene asymmetric electrochemical capacitors. *ACS Nano* **2010**, *4*, 5835–5842. [[CrossRef](#)] [[PubMed](#)]
104. Zhu, X. *Nanocarbon-Containing High Power Cathode for Rechargeable Hybrid Aqueous Battery*; UWSpace: Waterloo, ON, Canada, 2017.



© 2017 by the authors. Licensee MDPI, Basel, Switzerland. This article is an open access article distributed under the terms and conditions of the Creative Commons Attribution (CC BY) license (<http://creativecommons.org/licenses/by/4.0/>).